nature electronics

SUPPLEMENTARY INFORMATION

https://doi.org/10.1038/s41928-019-0257-7

In the format provided by the authors and unedited.

Wireless body sensor networks based on metamaterial textiles

**Xi Tian[1,6], Pui Mun Lee[1,6], Yu Jun Tan[2,3], Tina L. Y. Wu[4], Haicheng Yao[2], Mengying Zhang[1], Zhipeng Li[1], Kian Ann Ng[5], Benjamin C. K. Tee[2,3,5] and John S. Ho[1,3,5]*

[1]Department of Electrical and Computer Engineering, National University of Singapore, Singapore, Singapore. [2]Department of Materials Science and Engineering, National University of Singapore, Singapore, Singapore. [3]Institute for Health Innovation and Technology, National University of Singapore, Singapore, Singapore. [4]Department of Systems Design Engineering, University of Waterloo, Waterloo, Ontario, Canada. [5]The N.1 Institute for Health, National University of Singapore, Singapore, Singapore. [6]These authors contributed equally: Xi Tian, Pui Mun Lee. *e-mail: johnho@nus.edu.sg

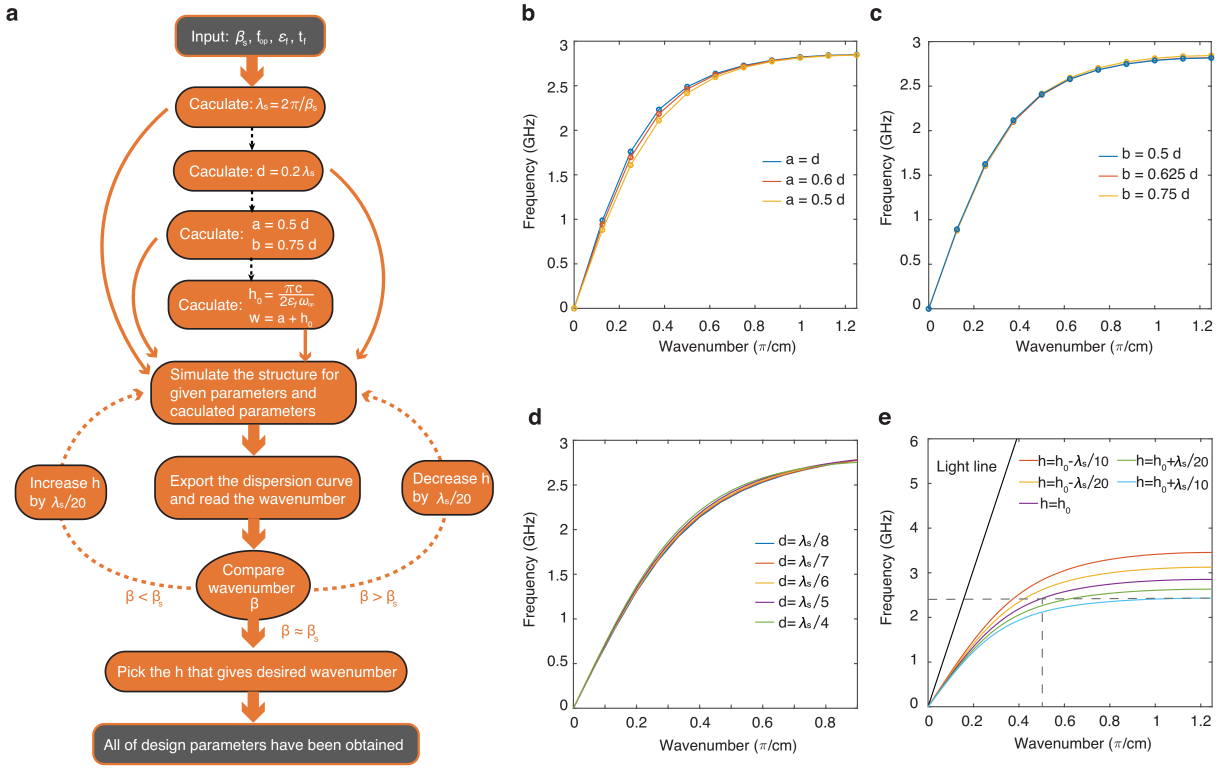

Supplementary Figure 1. Metamaterial textile design procedure. a, Schematic of the metamaterial textile design process. The geometrical parameters of the metamaterial structure are shown in Fig. 2a. **b-e**, Dispersion curves as the parameters a (**b**), b (**c**), d (**d**) and h (**e**) are varied. Within the design range, the dispersion curve is largely insensitive to the geometrical parameters except for h.

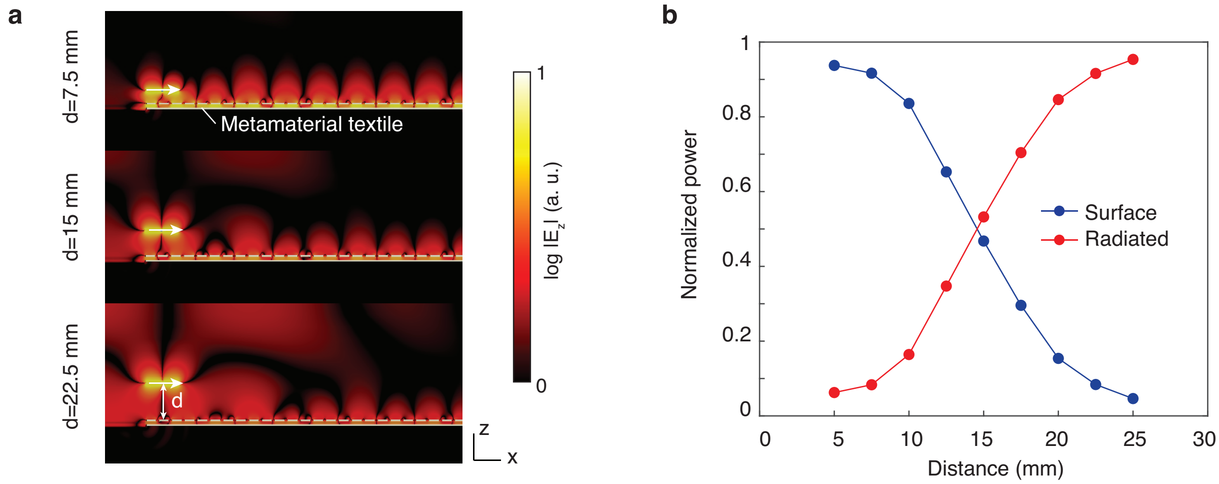

Supplementary Figure 2. **Excitation of surface modes versus radiative modes.** **a**, Electric field profile of the metamaterial textile with transmitter (horizontal electric dipole, 5 mm length) placed at varying distance d above the surface. **b**, Fraction of power transmitted into the surface modes and radiative modes as a function of d.

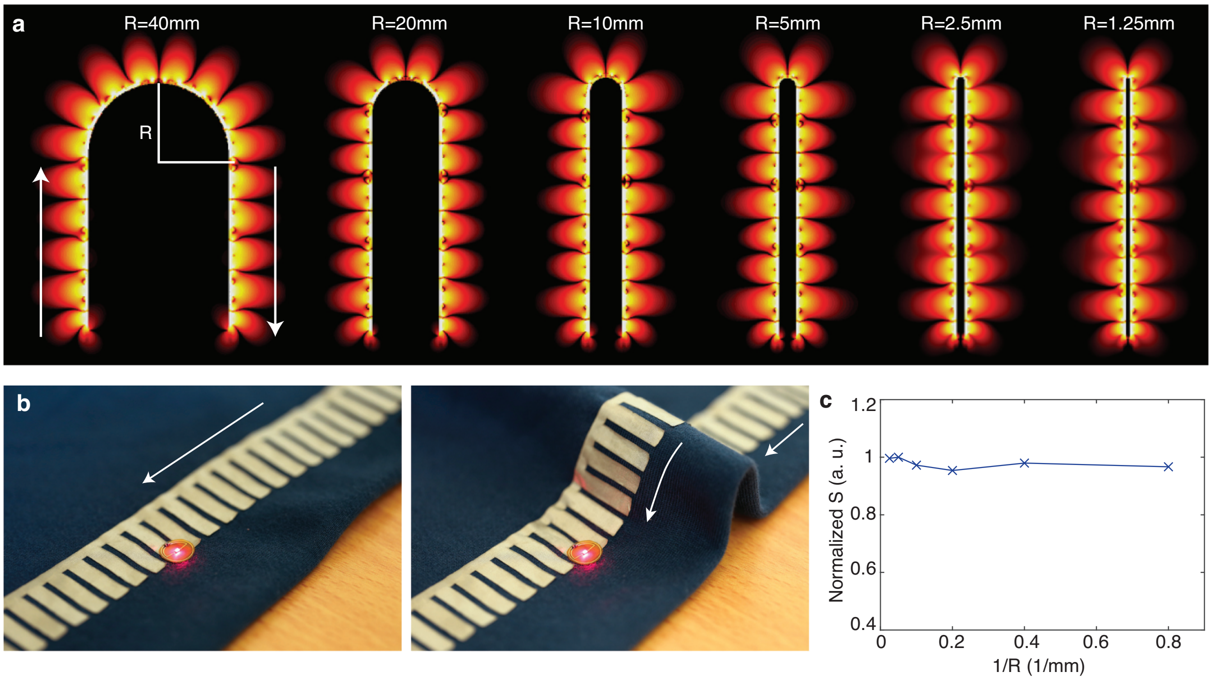

Supplementary Figure 3. **Propagation on U-shaped metamaterial textiles. a**, Full-wave simulations of the electric field at 2.4 GHz for U-shapes with varying radii-of-curvature R. The structure is excited at the bottom left point using a dipole placed 2 mm above the metamaterial textile. **b**, Photograph of a wireless energy harvester (powering a red LED) placed on a flat and creased metamaterial textile. **c**, Normalised Poynting vector (peak value) as a function of $1/R$ at the bottom right point of the structure symmetric to the excitation point.

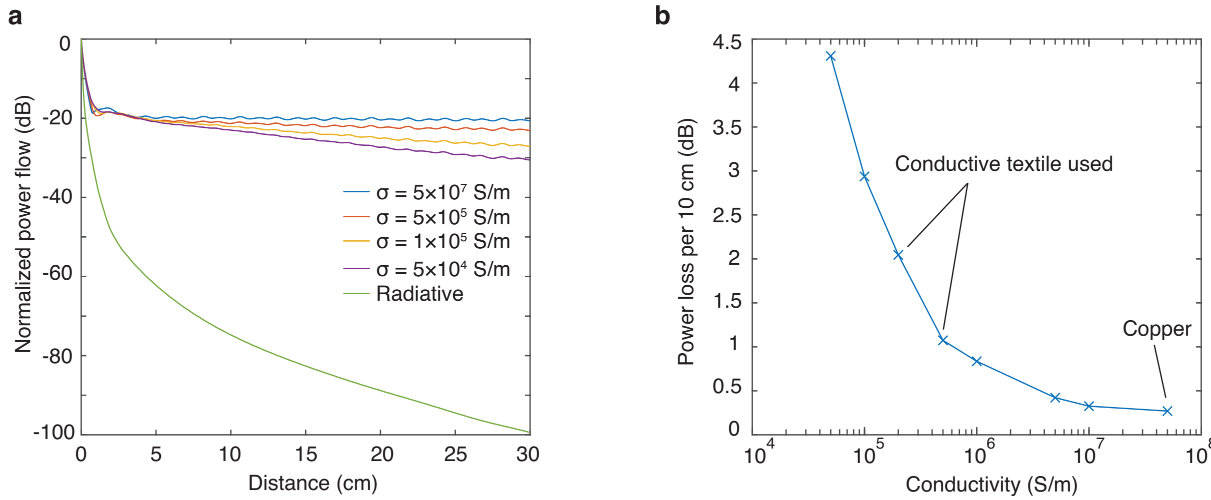

Supplementary Figure 4. **Propagation loss on metamaterial textiles.** **a**, Normalised power flow (Poynting vector) as a function of distance from the excitation point measured along a line 5 mm above the centre of the metamaterial textile comprised of textiles with varying conductivities. The curve labeled radiative shows the power flow as a function of distance in free-space. **b**, Power loss per 10 cm as a function of the textile conductivity. The conductive textiles used in this work have conductivities between 2×10^5 to 5×10^5 S/m.

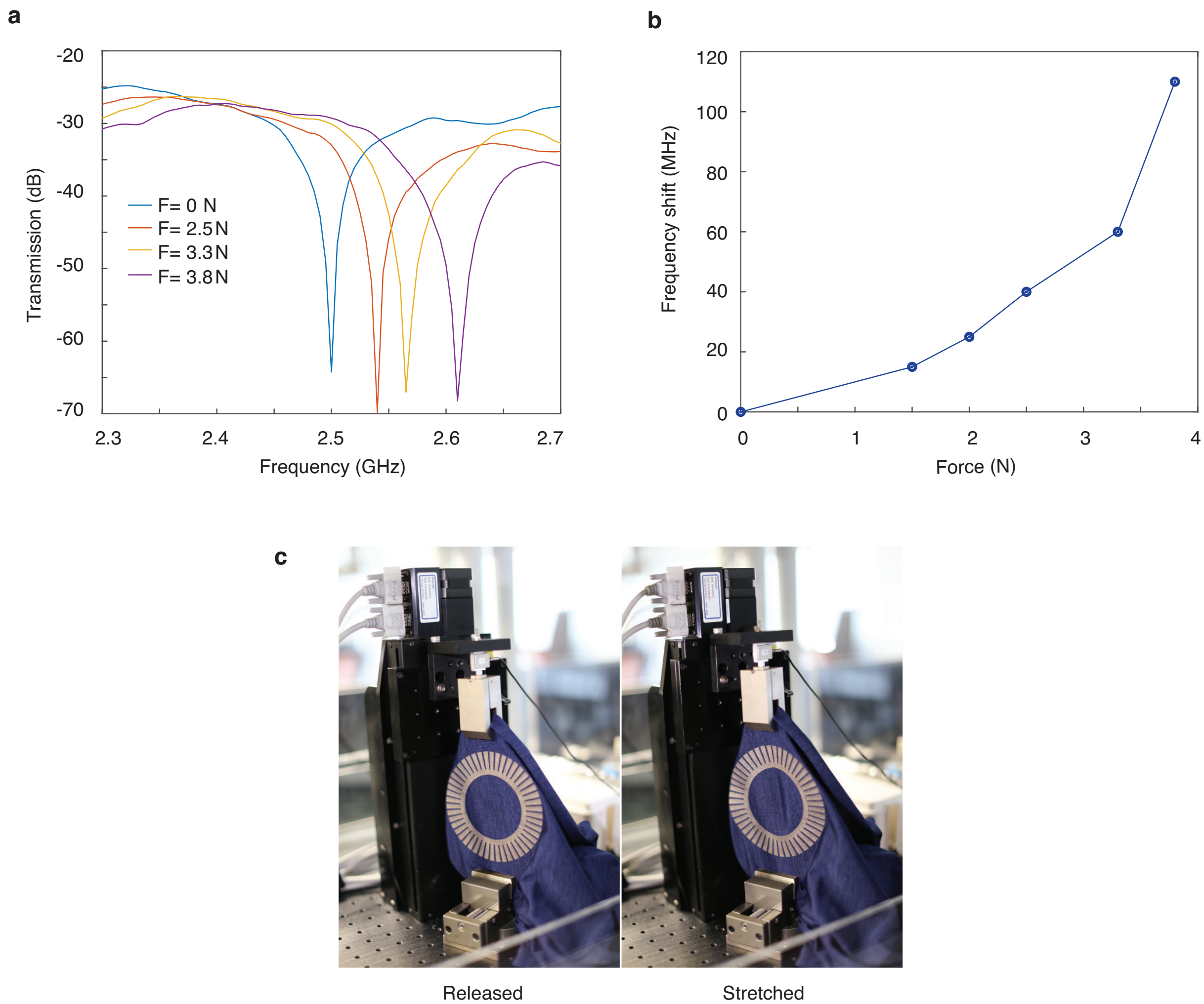

Supplementary Figure 5. **Resonance frequency of the ring resonator during textile stretching.** **a**, Transmission spectra measured between probes placed at two diametrically opposite points on the ring resonators as varying force is applied to the textile. **b**, Shift in resonant frequency as a function of the applied force. **c**, Image of the experimental setup.

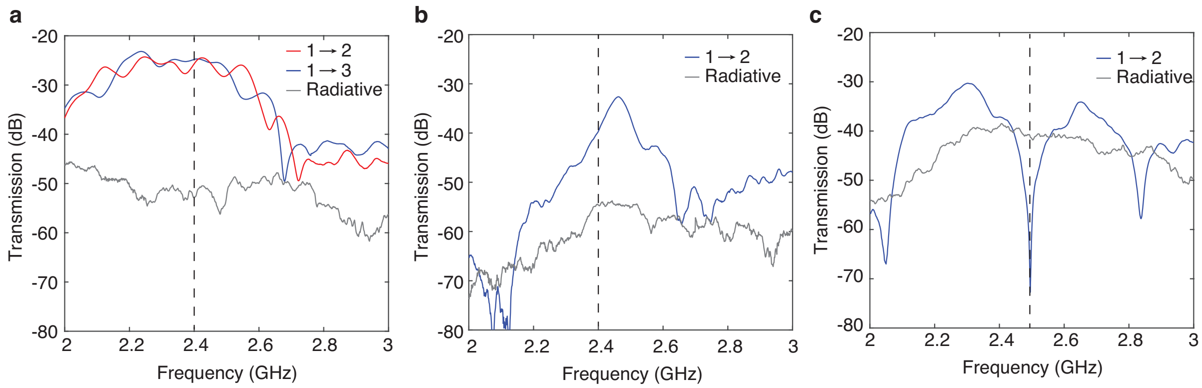

Supplementary Figure 6. **Transmission spectrum of radio-wave devices in free-space.** **a-c**, Transmission spectrum $|S_{nm}|$ for the (**a**) power divider, (**b**) antenna, and (**c**) ring-resonator devices measured in free-space without the human body. Measurements are performed using two antennas placed above the port locations labeled in Fig. 2.

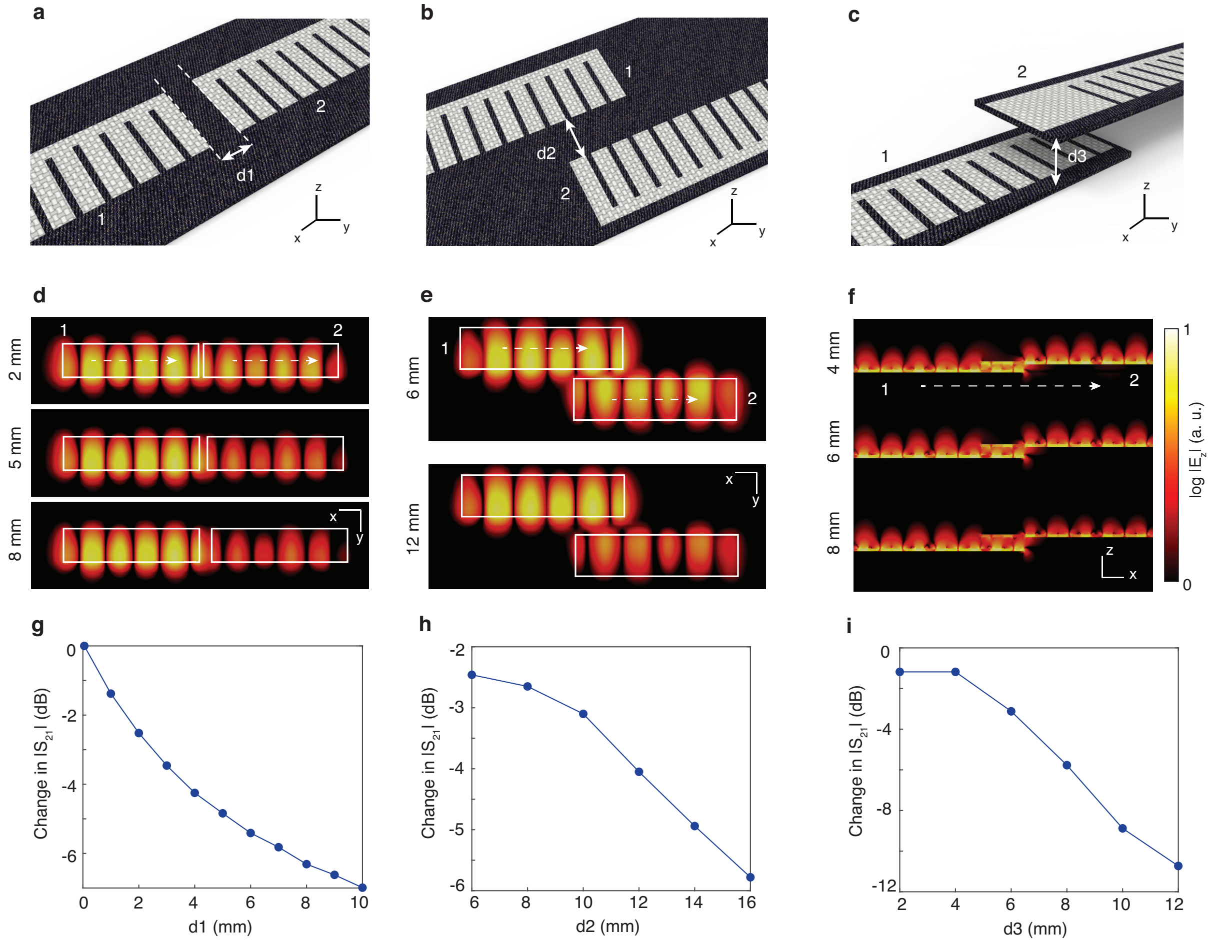

Supplementary Figure 7. **Radio surface plasmon propagation across discontinuities.** **a-c**, Discontinuities in the conductive structure of the metamaterial textiles in the (**a**) propagation direction x, (**b**) transverse direction y, and (**c**) vertical direction z. **d-f**, Amplitude of the normal component of the electric field $|E_z|$ for varying gap widths d_1 (**d**), d_2 (**e**), and d_3 (**f**). The transmitter (receiver) is a horizontal dipole placed 5 mm above the surface at position labeled 1 (labeled 2). **g-i**, Change in signal transmission $|S_{21}|$ as a function of gap width from $d_1 = 0$ (**g**), $d_2 = 6$ (**h**), and $d_3 = 2$ (**i**).

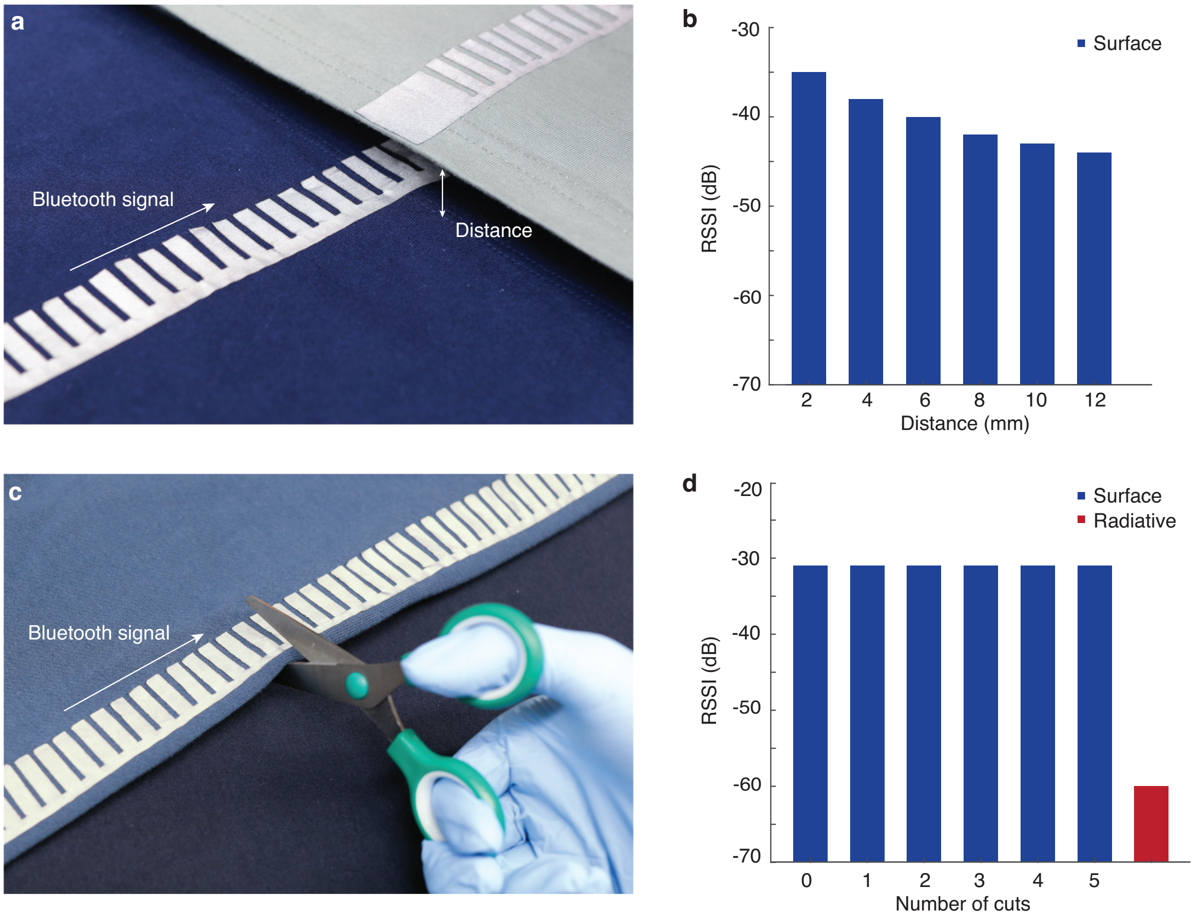

Supplementary Figure 8. **Robust Bluetooth signal propagation on metamaterial textiles.** **a**, Bluetooth signal propagation across a gap between two textiles. **b**, RSSI measured from a wireless receiver placed near the upper textile as the gap distance between the textiles is increased. **c**, Bluetooth signal propagation on textiles cut with scissors. **d**, RSSI as a function of numbers of cuts. Red bar shows RSSI measured in absence of the metamaterial textile.

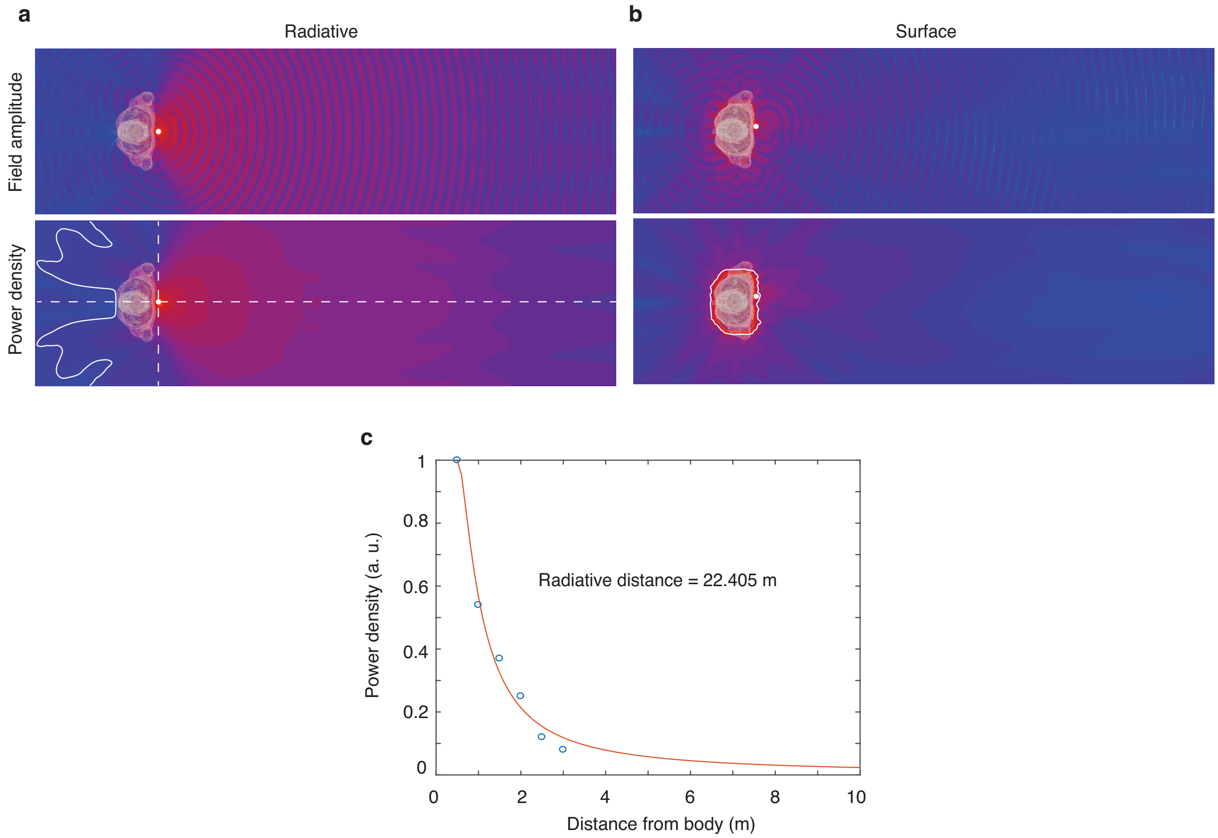

Supplementary Figure 9. **Secure wireless communication based on metamaterial textiles. a-b**, Instantaneous electric field amplitude and time-averaged power density S (logarithmic scale) for a dipole transmitter placed on the front (abdominal region) of a computational human body model without (radiative) (**a**) and with (surface) (**b**) the metamaterial textiles in Fig. 3a. The transmit power is the same in both configurations. The solid white lines show the power density contour line $S = S_{\text{back}}$ where S_{back} is the power density at the location of receiver placed on the back of the body. **c**, Power density radiated in front of the body along the dotted white line in (**a**). Solid line shows $\propto 1/d^2$ fit, where d is the distance from the body. The distance in front of the body at which $S = S_{\text{back}}$ is estimated to be 22.4 m.

a

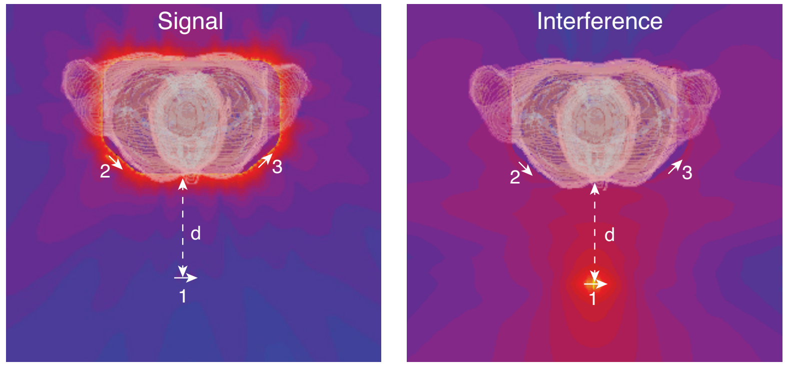

b

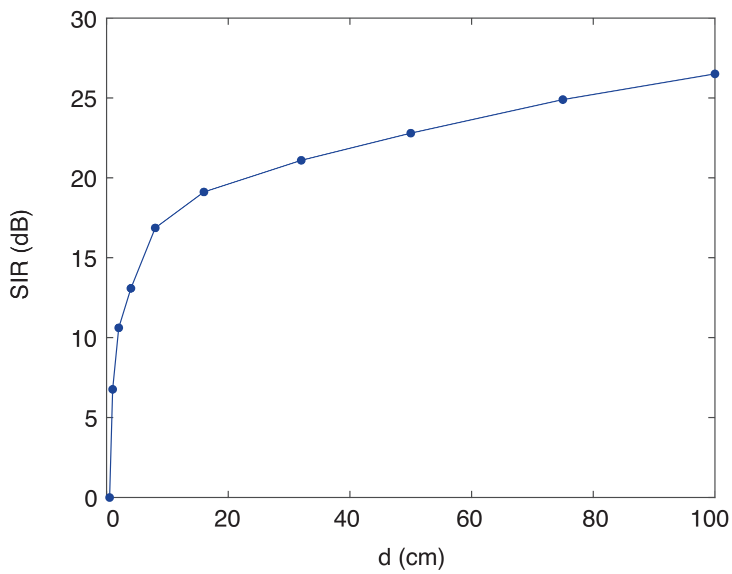

Supplementary Figure 10. **Interference from an external wireless transmitter. a**, Simulated time-averaged power density around the human torso during (left) wireless interconnection of two wearable devices (from device 2 to 3) and (right) wireless transmission from an interfering external wireless device (labeled 3). The human body model is wearing the metamaterial textiles shown in Fig. 3a and the interfering device is placed at distance d from the body. **b**, Signal-to-interference (SIR) ratio measured at the receiver (device 2) as a function of distance d of the interferer from the body. The transmit power of device 1 and device 2 are equal.

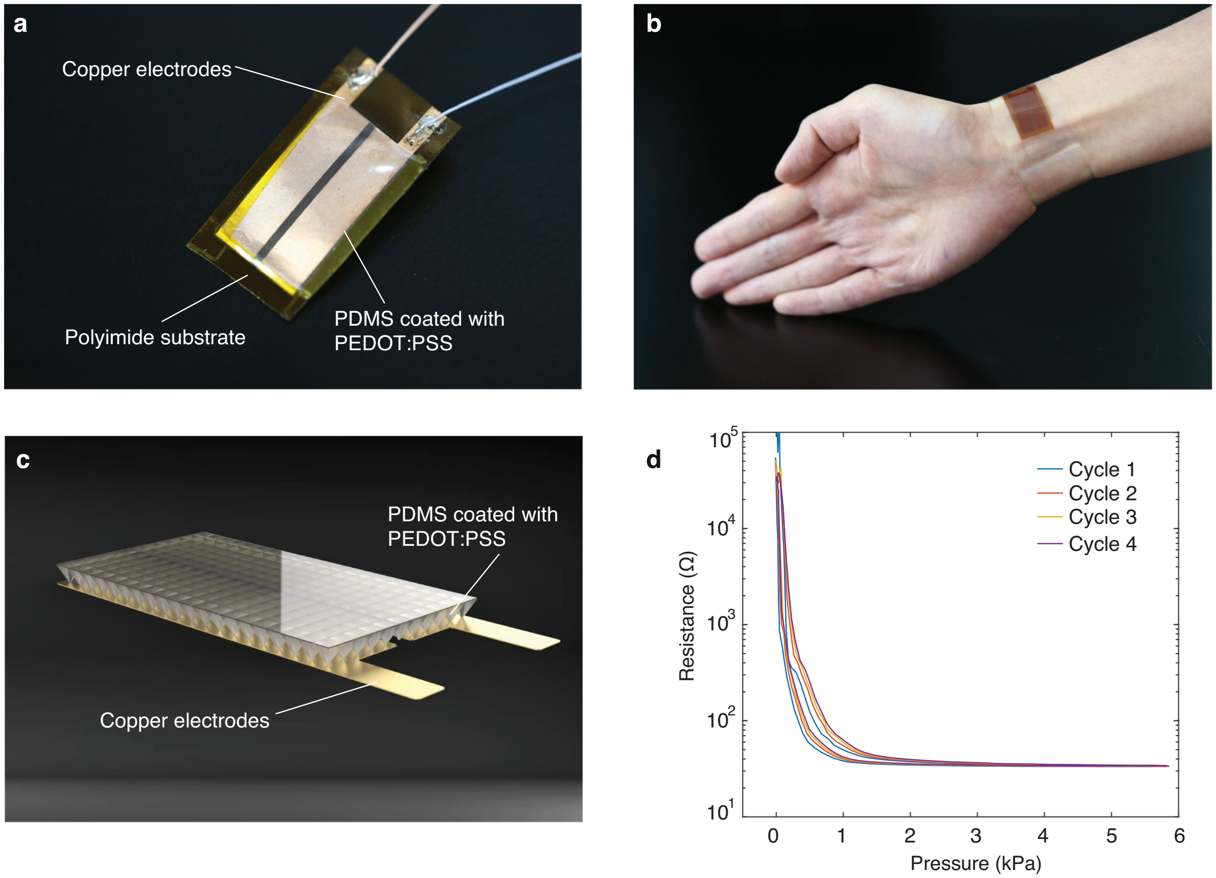

Supplementary Figure 11. **Microstructured pressure sensor for pulse detection.** **a**, Photograph of the integrated flexible pressure sensor. **b**, Photograph of the pressure sensor mounted on the wrist for pulse detection. The sensor is connected in parallel to a wirelessly powered LED to visualise pressure. **c**, Sensor design consisting of microstructured PDMS films coated with conductive polymer PEDOT:PSS. **d**, Resistance of the sensor as a function of applied pressure over 4 cycles.

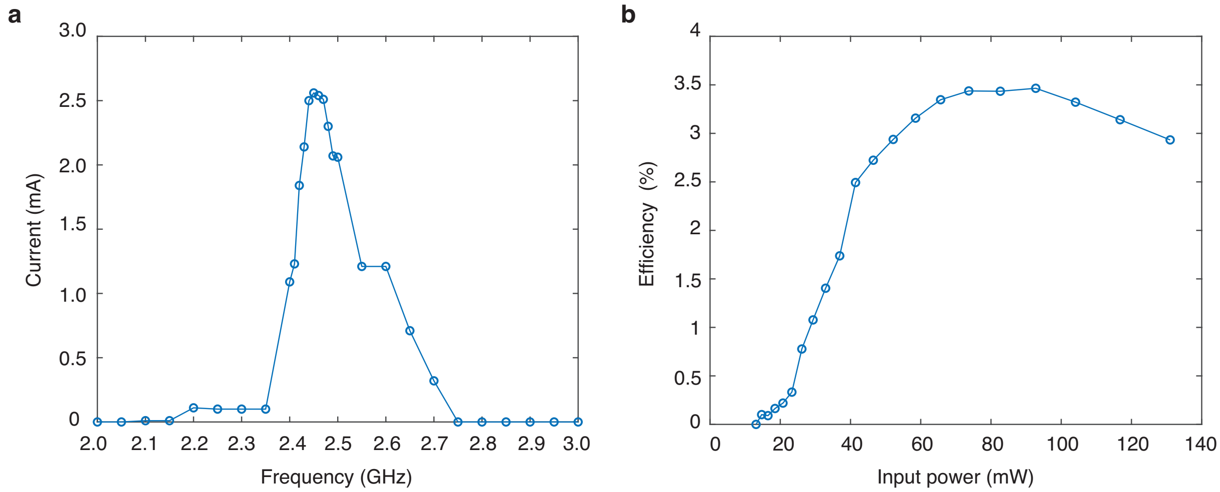

Supplementary Figure 12. **Wireless power transfer to light-emitting device.** **a**, LED current as a function of frequency at an input power of 100 mW to an antenna placed above the metamaterial textiles. **b**, Wireless power transfer efficiency, measured as the power delivered to the LED (including nonlinear rectifier losses), as a function of input power.

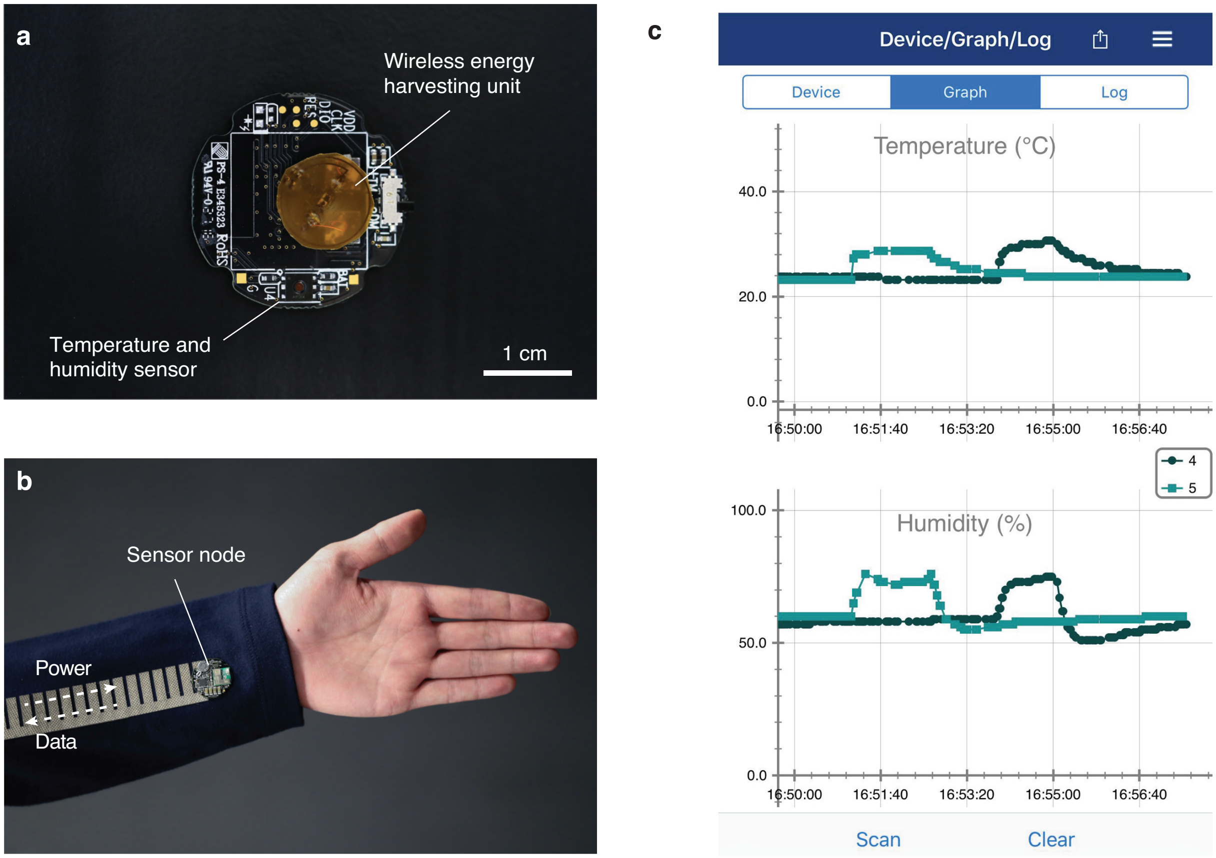

Supplementary Figure 13. **Battery-free, wirelessly powered Bluetooth sensor nodes.** **a**, Image of the back of the sensor node integrated with the custom wireless energy harvesting unit shown in Fig. 5b. The output of the energy harvesting unit is directly connected to the power management circuit of the Bluetooth module. **b**, Image of the sensor node placed on the wrist. The second sensor node is placed on the shoulder (Fig. 5d). **c**, Screenshot of smartphone application displaying data received from wireless sensor nodes on the shoulder and wrist (shown as nodes 4 and 5 respectively on the application) via propagation of Bluetooth signals along the metamaterial textile.

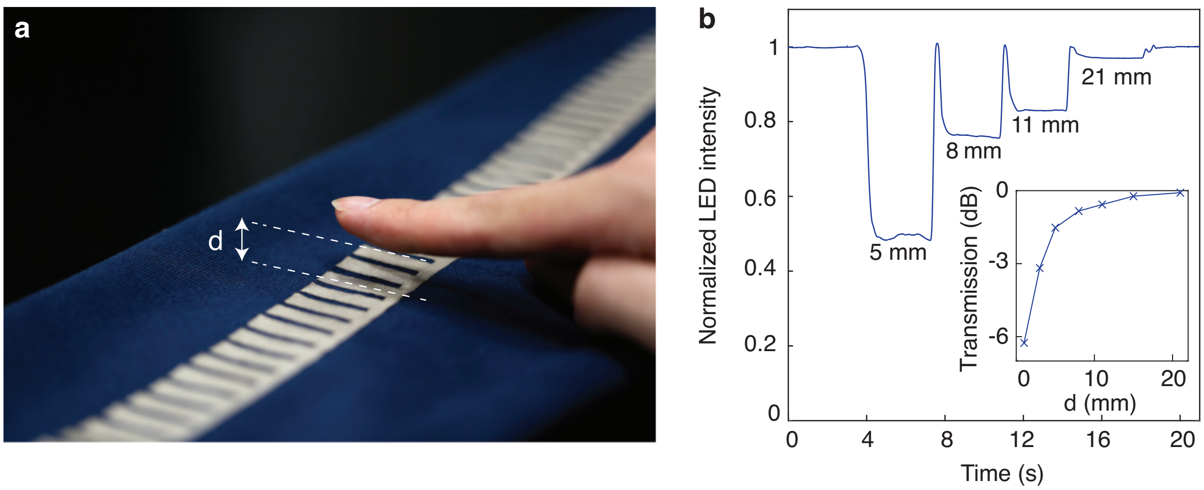

Supplementary Figure 14. **Textile-based wireless touch sensing.** **a**, Contactless sensing of finger proximity at distance d from the metamaterial textile. **b**, Sensing of finger proximity from the metamaterial textile. LED light intensity is modulated by the dependence of the transmission efficiency of the waveguide (inset) on finger distance.

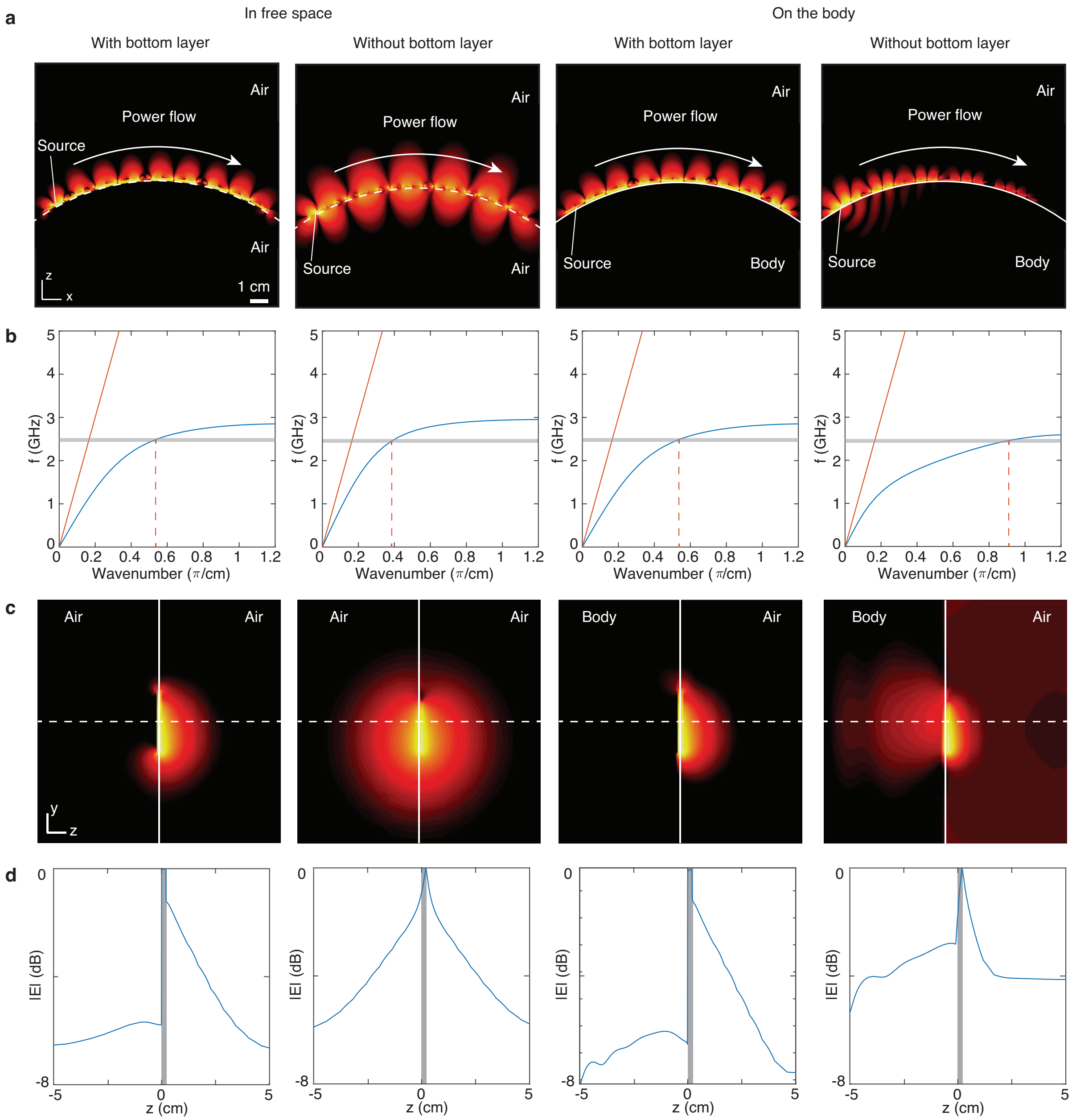

Supplementary Figure 15. Surface modes in free-space and on curved body surfaces. **a**, Amplitude of the electric field $|E_z|$ on the xz plane cutting through the centre of the structure on the body surface (modelled by cylinder with permittivity $\epsilon_{\text{body}} = 40$) with and without the bottom conductive fabric layer. The structure is excited by a dipole placed 2 mm above the clothing. **b**, Corresponding dispersion curves. **c**, Normalised field distribution on the yz plane. **d**, Field profile along the dashed line in (**c**) in free-space and above the body.

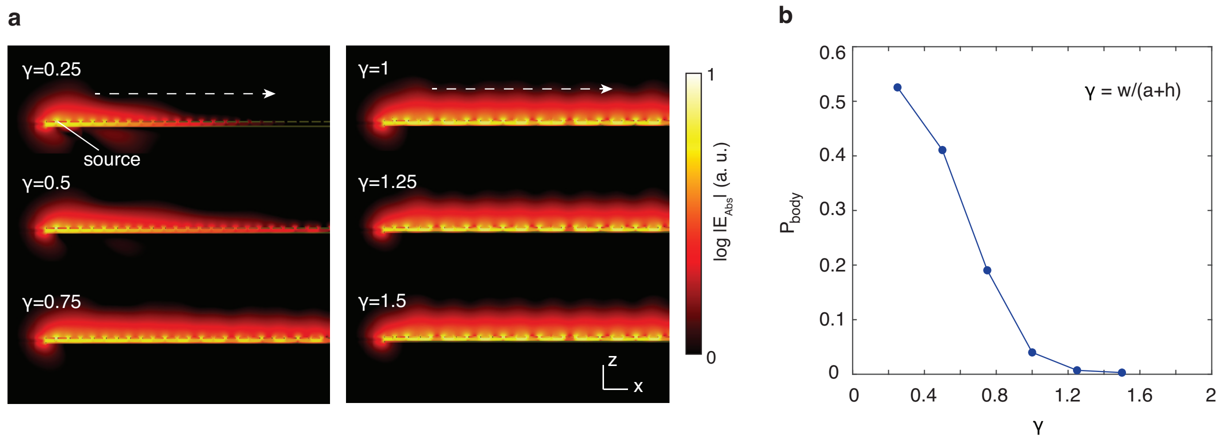

Supplementary Figure 16. **Design of metamaterial textiles for suppression of body interactions.** **a**, Time-averaged electric field amplitude on the metamaterial textile as the normalised width of the lower conductive layer $\gamma = w/(a+h)$ is varied. The metamaterial textile is excited on the left side by a horizontal electric dipole 5 mm above the surface. **b**, Fraction of power dissipated in the body P_{body} as a function of γ, normalised to the total dissipated power.